

# Understanding Masked Autoencoders From a Local Contrastive Perspective

Xiaoyu Yue<sup>1,2</sup> Lei Bai<sup>\*,2</sup> Meng Wei<sup>2,3</sup> Jiangmiao Pang<sup>2</sup> Xihui Liu<sup>3</sup>  
Luping Zhou<sup>1</sup> Wanli Ouyang<sup>2</sup>

<sup>1</sup>The University of Sydney   <sup>2</sup>Shanghai AI Laboratory   <sup>3</sup>The University of Hong Kong

## Abstract

*Masked AutoEncoder (MAE) has revolutionized the field of self-supervised learning with its simple yet effective masking and reconstruction strategies. However, despite achieving state-of-the-art performance across various downstream vision tasks, the underlying mechanisms that drive MAE’s efficacy are less well-explored compared to the canonical contrastive learning paradigm. In this paper, we first propose a local perspective to explicitly extract a local contrastive form from MAE’s reconstructive objective at the patch level. And then we introduce a new empirical framework, called Local Contrastive MAE (LC-MAE), to analyze both reconstructive and contrastive aspects of MAE. LC-MAE reveals that MAE learns invariance to random masking and ensures distribution consistency between the learned token embeddings and the original images. Furthermore, we dissect the contribution of the decoder and random masking to MAE’s success, revealing both the decoder’s learning mechanism and the dual role of random masking as data augmentation and effective receptive field restriction. Our experimental analysis sheds light on the intricacies of MAE and summarizes some useful design methodologies, which can inspire more powerful visual self-supervised methods.*

## 1. Introduction

Recently, self-supervised learning has seen significant progress in the field of computer vision with two dominant paradigms, *i.e.*, Contrastive Learning, and Masked Image Modeling. The Contrastive Learning methods [4–8, 11, 14, 15] benefit from learning invariance by contrasting positive and negative image pairs, which are constructed from random data augmentations. On the other hand, the Masked Image Modeling paradigm [2, 13, 16, 34], which is inspired by Masked Language Modeling in the field of Natural Language Processing, involves randomly masking a portion of an input image and learning to reconstruct the

missing pixels based on the visible part. Recent studies have shown that the ViT features pretrained with Masked Image Modeling have achieved competitive or even better performance than those with Contrastive Learning when finetuning on downstream tasks.

As a typical MIM method, Masked AutoEncoder (MAE) [16] represents a significant breakthrough in visual representation learning, as it paves the way for harnessing the potential of masked autoencoding techniques in vision. MAE adopts a simple asymmetric encoder-decoder architecture and is pretrained to reconstruct masked images generated through aggressive masking, with a large mask ratio of up to 75%. However, despite the efficiency and simplicity of MAE, the implicit generative way of pretraining presents a challenge to decipher the exact factors contributing to its performance. In contrast, the Contrastive Learning paradigm, which has well-defined formulations and explicit supervision of the encoded features, is more comprehensively understood in the field. Given the existence of these two distinct paths in SSL, we believe that gaining a better understanding of MAE can drive SSL toward a unified and more effective direction.

Recent works [19, 36] have provided a theoretical framework to approximate MAE with contrastive learning, which is promising as it allows for leveraging the insights gained from contrastive learning to interpret MAE. While the mathematical approximations and assumptions made in these works provide a good starting point, explicit empirical evaluation at the operational level is still lacking. To bridge the gap, we first take a novel local perspective to interpret MAE. Specifically, we propose reformulating MAE’s training objective based on image patches, rather than the entire image. This reformulation enables us to directly decompose MAE’s reconstructive objective into a combination of reconstructive and contrastive objectives. More importantly, based on this decomposition, we propose an empirical framework, namely Local Contrastive MAE (LC-MAE), to analyze both the reconstructive and contrastive aspects of MAE. LC-MAE not only preserves MAE’s state-of-the-art performance on downstream tasks but also unveils the explicit local contrastive form of MAE. It uses three explicit

\*Corresponding author: bailei@pjlab.org.cn.

token-based loss functions: a reconstruction loss, a cross-view contrastive loss, and an in-view contrastive loss. The cross-view loss ensures that, for a given image, token features in the same position but different random masks are locally similar, revealing that MAE actually learns invariance to random masking. The in-view loss ensures the consistency of the distribution of the output features and the input image, which effectively prevents the collapse of MAE.

Apart from connecting MAE to contrastive learning, we also deeply investigate how each component of MAE, *i.e.*, the autoencoder and the random masking, contributes to its success. For the autoencoder, we focus on analyzing the decoder’s behaviors, and find that the decoder primarily utilizes positional information in the shallow layers, and gradually learns semantic information as going to deeper layers. This demonstrates that a deep decoder is essential for learning rich semantic representations. For the random masking strategy, it serves two purposes: (1) data augmentation; (2) restricting the effective receptive field of Vision Transformers, which turns out to be crucial for MAE’s effectiveness on downstream tasks. Surprisingly, we found that solely restricting the receptive field is enough to improve downstream finetuning performance.

We hope our analysis of MAE will inspire future research in the field of visual representation learning.

## 2. Related Work

**Contrastive learning.** As the dominant self-supervised representation learning paradigm in the field of computer vision, contrastive learning [4, 7, 11, 14, 15] learns invariance by comparing random views. A representative work in this domain is SimCLR [6], which learns semantic representations by maximizing the similarity between different views derived from the same image within the latent space. MoCo v3 [8] explores the pretraining of vision transformers through the methodology of contrastive learning. DINO [5] explores new properties of self-supervised vision transformers.

**Masked Image Modeling.** In recent years, the development of Vision Transformers [10, 12, 30] has significantly encouraged the application of Masked Image Modeling (MIM). Originating from Masked Language Modeling, MIM has achieved impressive results in visual self-supervised representation learning. BEiT [2] maps image patches into visual tokens using d-VAE [27] and predicts these visual tokens based on the masked images. SimMIM [34] attempts to simplify the algorithmic process of MIM by directly using the original image pixels as the target. MAE [16] employs an encoder-decoder framework to perform image reconstruction tasks. IBOT [38], CAE [9], and CMAE [17] try to combine contrastive learning and MIM.

**Understanding MAE.** Despite the simplicity and efficacy

of MAE, there is a paucity of work dedicated to understanding and analyzing its inner mechanism. Many existing works [20, 21, 23] focus on improving MAE based on intuitive understanding. Cao et al. [3] primarily focuses on the role of self-attention within the MAE framework. Kong et al. [18] abstracted MAE as a hierarchical latent variable model, thereby analyzing the mechanism through which MAE learns semantic information. Park et al. [26] conducted a comparative analysis of the behavioral differences between the MIM and contrastive learning. Kong and Zhang [19] and Zhang et al. [36] reformulate MAE as contrastive learning, sharing similar motivation with us. However, they both consider masked patches and visible patches as two views for global contrastive learning, while we demonstrate that MAE actually conducts contrastive learning between local regions on the masked image.

## 3. A Local Perspective for MAE

In this section, we introduce the local contrastive learning form of MAE, which is a more accessible way for understanding the intrinsic mechanisms of MAE. This contrastive form conceptually elaborates that MAE acquires semantic representations by aligning features at the patch level. Specifically, we first provide a brief revisit of MAE in Section 3.1, and then we show how to reformulate MAE in Section 3.2. Finally, in Section 3.3, we introduce a contrastive learning approach derived from MAE, termed Local Contrastive MAE (LC-MAE). Empirically, we demonstrate that using only patch-level contrastive losses can also learn features similar to those acquired by masked image modeling.

### 3.1. A brief revisit of MAE

Masked AutoEncoders (MAE) [16] is a straightforward yet efficacious self-supervised method for pretraining Vision Transformers (ViT) [10, 30]. It learns rich hidden representations by masking a large portion of the image and reconstructing the masked patches based on the visible patches.

Formally, given an input image, MAE first partitions it into  $n$  non-overlapping patches, denoted as  $x = \{x_i\}_{i=1}^n$ . Then, the  $n$  patches are split into two complementary subsets with a random binary mask  $m \in \{0, 1\}^n$ : the *visible patches*  $x^v = x[1-m]$  and the *masked patches*  $x^m = x[m]$ . MAE adopts an encoder-decoder architecture:  $h = g \circ f$ . The encoder  $f(\cdot)$  encodes the visible patches into the visible token representations  $z$ :  $z = f(x^v)$ . Then the visible tokens  $z$  are fed into the decoder  $g(\cdot)$ . Meanwhile, all the masked positions will be filled with a shared learnable mask token  $e_M$ . Both  $z$  and  $e_M$  are added with positional embeddings. Subsequently, the resulting token sequence is used to reconstruct the original pixels of the mask tokens. MAE employs the Mean Squared Error (MSE) loss function for

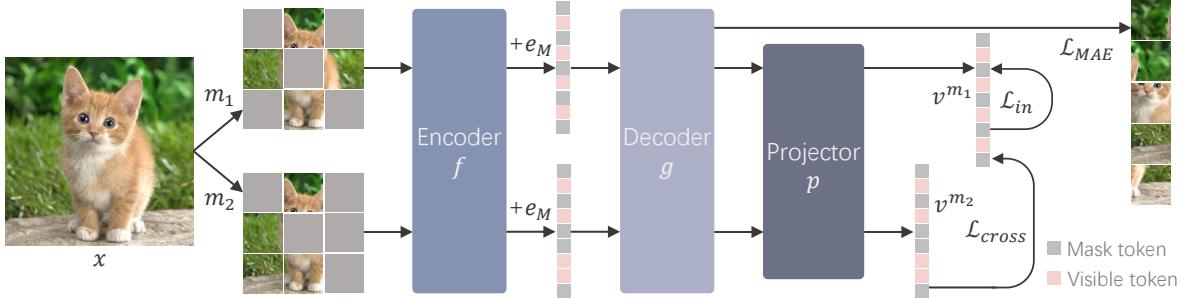


Figure 1. The overall pipeline of LC-MAE. The input image  $x$  is masked by  $m_1$  and  $m_2$ , yielding two augmented views. Then the two views are separately fed into the MAE model and projector  $p$ , resulting in feature vectors  $v^{m_1}$  and  $v^{m_2}$ . In addition to the MAE’s reconstruction loss  $\mathcal{L}_{MAE}$ , two contrastive losses,  $\mathcal{L}_{cross}$  and  $\mathcal{L}_{in}$ , are computed using  $v^{m_1}$  and  $v^{m_2}$ .

pretraining:

$$\mathcal{L}(x, m) = \sum_{i=1}^n m_i \cdot \|h(x, m)_i - x_i\|^2, \quad (1)$$

$$h(x, m) = g(f(x[1 - m])).$$

In the original implementation of MAE, the decoder output is  $l_2$ -normalized, and a high mask ratio (e.g. 75%) is commonly applied to generate the random mask  $m$ .

### 3.2. Reformulating MAE as Local Contrastive Learning

Previous research [19, 36] has demonstrated that MAE can be better understood from the perspective of contrastive learning. Although they approximate the formulation of MAE with the global alignment loss in contrastive learning, their interpretation of MAE still relies on certain assumptions. We find that the MAE naturally maps different masked tokens to similar content, hence a local perspective may be more suitable to describe MAE.

During the entire training process of MAE, for a position  $j$  in an input image  $x$ , there exist two different training iterations that construct the masked patch  $x_j$  with two randomly generated masks  $m_a$  and  $m_b$  (where  $m_a \neq m_b$ ).

Disregarding that  $m_a$  and  $m_b$  are generated in different iterations, we view  $m_a$  and  $m_b$  as two data augmentations performed on the same image as in contrastive learning. Hence, from the local perspective (i.e., the image patch level), we rethink the training objective of MAE  $\mathcal{L}(x, m)$  w.r.t. two random data augmentations  $m_a$  and  $m_b$  and the  $j$ -th patch as:

$$\begin{aligned} \mathcal{L}(x, m)_j &= \|h(x, m_a)_j - x_j\|^2 \\ &= \|(h(x, m_a)_j - h(x, m_b)_j) + (h(x, m_b)_j - x_j)\|^2 \\ &= \|(h(x, m_a)_j - h(x, m_b)_j) + e_{pred}(j|m)\|^2, \end{aligned} \quad (2)$$

where  $e_{pred}(j|m)$  is the prediction error:

$$e_{pred}(j|m) = h(x, m)_j - x_j. \quad (3)$$

It represents the reconstruction objective of MAE: the decoder output at the position  $j$  with random masking operation  $m$  should always approximate the invariant image patch value  $x_j$ .

The first term of Eq. 2 ( $h(x, m_a)_j - h(x, m_b)_j$ ) can be regarded as a *patch-level contrastive objective*: align the local patch features in two augmented views.

Considering that Eq. 2 is just a conceptual reformulation of MAE, as the two random augmentations  $m_a$  and  $m_b$  do not actually occur in the same training iteration, we further provide a reformulation based on the masked image patches in a single forward of MAE.

Similarly, we rethink  $\mathcal{L}(x, m)$  w.r.t. two different masked positions  $i$  and  $j$  of an input image  $x$  as:

$$\mathcal{L}(x, m)_i = \|h(x, m)_i - x_j + x_j - x_i\|^2 \quad (4)$$

Substituting  $x_j$  with  $h(x, m)_j - e_{pred}(j|m)$  from Eq. 3

$$\begin{aligned} \mathcal{L}(x, m)_i &= \|(h(x, m)_i - (h(x, m)_j - e_{pred}(j|m)) \\ &\quad - (x_i - x_j))\|^2 \\ &= \|(h(x, m)_i - h(x, m)_j) - (x_i - x_j) \\ &\quad + e_{pred}(j|m)\|^2. \end{aligned}$$

The first term requires that the difference between the decoder outputs at positions  $i$  and  $j$ , i.e.,  $(h(x, m)_i - h(x, m)_j)$ , should approximate their pixel difference  $(x_i - x_j)$ . This can also be regarded as the contrastive objective at the patch level with the distance between the masked patches as an additional margin.

So far, we have separated the local contrastive form of MAE from its reconstructive form, in both Eq. 2 and Eq. 4. Just as pointed out in Zhang et al. [36], MAE’s reconstruction ability is not enough to explain the efficacy of MAE, since pretraining with vanilla autoencoder performs much worse than MAE. Hence, we believe that the derived local contrastive form, which indicates that *MAE implicitly aligns local features*, may help uncover its underlying mechanism.

In the following section, we will introduce an architecture that transforms the implicit local contrastive form of MAE into an explicit form, in order to empirically evaluate the impact of each aspect of MAE.

### 3.3. Explicit Local Contrastive Form of MAE

Based on Eq. 2 and Eq. 4, we summarize three possible training objectives of MAE:

- i Patch reconstruction.
- ii The first term of Eq. 2, aims to minimize the patch token embedding distance in different views of an image.
- iii The first term of Eq. 4, aims to minimize the discrepancy between the distribution of the output token embeddings and the distribution of the input image patches.

However, the framework of MAE makes it impossible to explicitly perform ablative studies on each individual training objective. Hence, we design a simple framework to instantiate the local contrastive learning form of MAE into explicit loss functions, namely Local Contrastive MAE (LC-MAE).

The overall pipeline of LC-MAE is shown in Figure 1. Compared to MAE, the input of LC-MAE becomes two masked views of the same image. It has three loss functions: the reconstruction loss  $\mathcal{L}_{MAE}$  (w.r.t. objective i); the cross-view loss  $\mathcal{L}_{cross}$  (w.r.t. objective ii); and the in-view loss  $\mathcal{L}_{in}$  (w.r.t. objective iii). LC-MAE employs the same encoder and decoder architecture as MAE. Hence, the reconstruction loss  $\mathcal{L}_{MAE}$  remains consistent with that of MAE. For calculating contrastive losses  $\mathcal{L}_{in}$  and  $\mathcal{L}_{cross}$ , we introduce an extra fully connected layer as the projector ( $p(\cdot)$ ) to produce the output vector  $v = p(h(x, m))$ .

In the application of the cross-view loss  $\mathcal{L}_{cross}$ , the model utilizes two random masks,  $m_1$  and  $m_2$ , to mask the input image  $x$ . The resulting output vectors for the two masked views are denoted as  $v^{m_1}$  and  $v^{m_2}$ , respectively.  $\mathcal{L}_{cross}$  maximizes the cosine similarity between the paired vectors at positions that are simultaneously masked in two views. This operation is equivalent to the mean squared error of  $l_2$ -normalized vectors [14], formally:

$$\mathcal{L}_{cross} = \sum_i^n (m_{1,i} \cdot m_{2,i}) \cdot (1 - \cos(v_i^{m_1}, v_i^{m_2})), \quad (5)$$

where  $\cos(\cdot, \cdot)$  denotes the cosine similarity, and  $i$  is the patch index.

The in-view loss  $\mathcal{L}_{in}$  is calculated within a single masked view. It leverages the cosine similarity matrix of the input image patches  $x$  as the supervision for the output tokens, in order to explicitly align these two distributions. The mean absolute error between the cosine similarity matrix of output tokens  $v$  and the original image patches is

Setting	$\mathcal{L}_{MAE}$	$\mathcal{L}_{cross}$	$\mathcal{L}_{in}$	FT Acc(%)
(a)	✓	✓	✓	83.0
(b)	✓			82.9
(c)		✓		Collapse
(d)			✓	82.2
(e)	✓	✓		83.1
(f)	✓		✓	82.8
(g)		✓	✓	82.5

Table 1. Finetuning accuracy (FT Acc) of LC-MAE under different settings.

calculated as:

$$\mathcal{L}_{in} = \sum_{i \neq j}^n (m_i \cdot m_j) \cdot |\cos(v_i, v_j) - \cos(x_i, x_j)|. \quad (6)$$

The overall loss of LC-MAE is the sum of these three losses:  $\mathcal{L}_{MAE} + \mathcal{L}_{in} + \mathcal{L}_{cross}$ .

We pretrain the LC-MAE on ImageNet with a mask ratio of 75% for 100 epochs. And then supervised finetuning the model on ImageNet for an additional 100 epochs. To shorten the pretraining duration, we set the depth of the decoder to 2.

**Ablation Study.** We conducted ablation studies to demonstrate the effectiveness of each loss function and analyzed the key success factors of MAE. As shown in Table 1:

- (1) Setting (a) is LC-MAE, which incorporates all three losses, showing a slight improvement compared to Setting (b), *i.e.*, the original MAE (reconstruction loss only). This indicates that LC-MAE retains the effectiveness of MAE.
- (2) The reconstruction loss consistently improves performance, with gains of 0.5% in setting (a) versus (g), and 0.6% in setting (f) versus (d). Hence, the reconstruction loss is indeed simple yet effective.
- (3) The cross-view loss leads to performance gains of 0.3% in setting (g) versus (d), and 0.2% in setting (a) versus (f). In MAE, the cross-view loss is implicitly realized during the training process, while in LC-MAE, its explicit implementation enhances the capacity to learn semantic representations.
- (4) The in-view loss leads to a slight performance decline of 0.1%, possibly due to a suboptimal similarity matrix.
- (5) It is noteworthy that setting (g), even without the use of reconstruction loss, still achieves a finetuning accuracy of 82.5%, corroborating the intrinsic nature of contrastive learning implicitly performed by MAE, and hinting at the potential of pure contrastive learning.

**How MAE avoids Feature Collapse.** From the ablation study, we can also explain why MAE doesn't suffer from feature collapse when only aligning the positive pairs. Since LC-MAE inherits the network architecture of MAE and



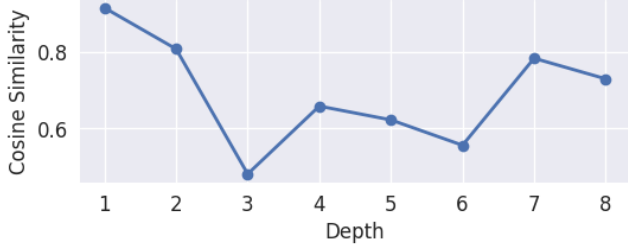


Figure 2. The average attention similarity for each decoder layer, indicates the degree of reliance on positional information.

does not employ techniques such as extra predictor, momentum encoder, or stop-gradient to prevent model collapse, using only the cross-view loss (setting (c) in Table 1) leads to collapse into a constant point. When the model is equipped with the in-view loss (setting (g)) or reconstruction loss (setting (e)), it is able to avoid collapsed solutions. This indicates that MAE actually employs two methods to avoid collapse: 1) assigning a unique target value for each predicted value; and 2) ensuring that the output has a distribution similar to that of the input image. In both methods, collapse would result in large loss values.

#### 4. Component Analysis of MAE

In this section, based on the reformulation of MAE, we dissect the role of two main components of MAE: autoencoder and masking, and delve into what contributes to its success as a self-supervised framework. Within the autoencoder, the encoder serves as the network utilized for downstream tasks, whereas the decoder, which reconstructs masked tokens back into pixels, is the most innovative part of MAE. For this reason, we focus on the significance of the decoder, and explore the decoding process in Section 4.1, unveiling how MAE learns semantic features and conducts local contrastive learning. Subsequently, the role of masking is discussed in Section 4.2, where we discover that aside from serving as data augmentation and providing a learning target for MAE, masking also effectively controls the network’s effective receptive field, which is one of the reasons for MAE’s strong performance in downstream tasks.

##### 4.1. Decoder

To uncover the inner mechanisms of MAE, it’s critical to comprehend the decoder’s role in helping the encoder learn rich hidden representations in a generative manner, even though the decoder will be discarded after pertaining.

We noticed that the mask token  $e_M$  is shared across all masked positions, with only the added position embeddings varying. Nevertheless, considering the distinctive content decoded from various masked positions, we speculate that the decoding process of MAE might be initially guided by positional information.

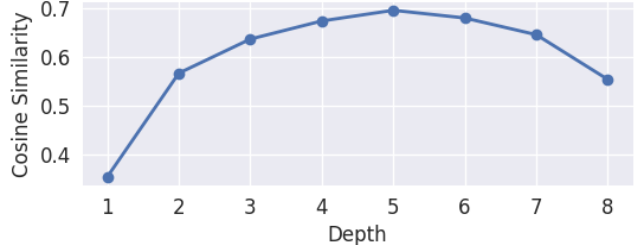


Figure 3. The average cosine similarity between the DINO features and the features of each decoder layer, quantifies the semantic richness of decoder features.

To examine this assumption, we conduct statistical analysis on the attention maps from different decoder layers using the validation set of ImageNet-1K. To reduce the complexity of the analysis, we deliberately mask all the images with identical random binary masks (*i.e.*, masked positions are kept the same). Let  $\mathcal{I}$  denote the set of all images, for the  $l$ -th decoder layer, we extract the attention maps from all masked positions of the  $i$ -th image, defined as  $A_{l,i} \in \mathbb{R}^{k \times h \times n}$  with  $k$ ,  $h$ , and  $n$  denote the number of mask tokens, the number of heads, and the number of patches, respectively. Then we compute the cosine similarity of each attention map pair  $\cos(A_{l,i}, A_{l,j})$  and average the similarity scores across the whole image set:

$$S_l^{attn} = \frac{\sum_{i \neq j}^{|\mathcal{I}|} \cos(A_{l,i}, A_{l,j})}{|\mathcal{I}|(|\mathcal{I}| - 1)}, \quad (7)$$

where  $|\mathcal{I}|$  is the number of images, and  $S_l^{attn}$  is the average cosine similarity of attention maps at  $l$ -th decoder layer. A higher similarity means the decoder layer relies more on invariant features shared across images, *i.e.*, the positional information.

As shown in Figure 2, the average attention map similarity across all images is the highest at the first decoder layer (up to 0.9) and lowest at the third layer. The average cosine similarity of the first two layers is significantly higher than that of the subsequent layers. This suggests that **positional information is learned primarily at the shallower layers.**

Then the intriguing question is: *How does the decoder acquire the semantic information?* Inspired by CutLER [31], LOST [29], and TokenCut [32], we use features extracted by DINO [5] as an indicator to measure the semantic richness of each decoder layer. DINO [5] is a widely adopted self-supervised vision model, which produces features that appear to contain explicit information about semantic segmentation. Following CutLER [31], we calculate the cosine similarity between patch features within the same layer and use the normalized cosine similarity matrix as the similarity weight  $W$ , which is a  $n \times n$  symmetrical matrix. Then, by computing the average cosine similarity between the similarity weights of each decoder layer and those from

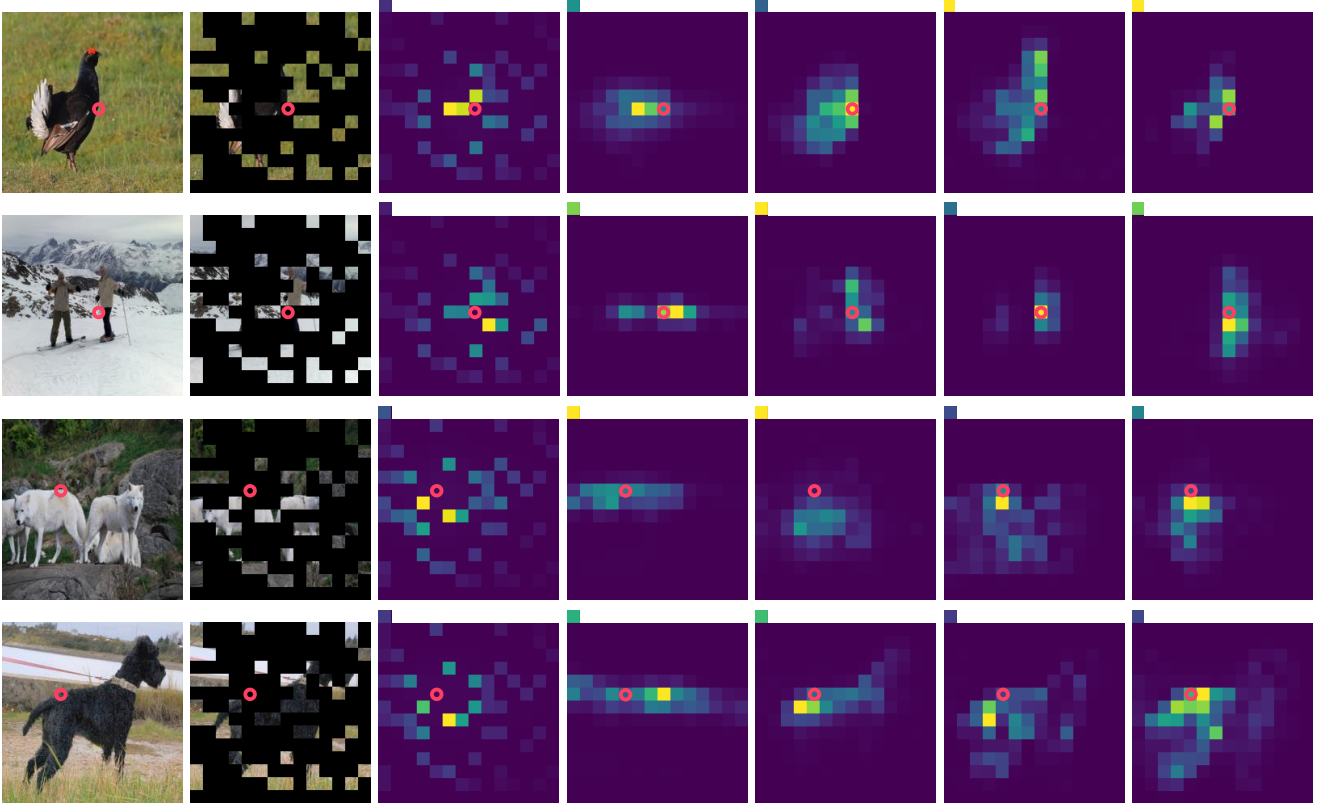


Figure 4. Visualization of attention maps from decoder layers. From left to right: input images, masked images, and attention maps of the 1-st, 2-nd, 3-rd, 5-th, 8-th decoder layers. The red circles ( $\odot$ ) denote the masked tokens serving as queries. The first two rows and the last two rows show mask tokens at different positions. The block in the top-left of each attention map is the weight for the [CLS] token.

the final layer of DINO, we can quantify the extent to which the decoder utilizes semantic information. Formally:

$$S_i^{sim} = \frac{\sum_i^{|I|} \cos(W_i^{dino}, W_{l,i}^{dec})}{|I|}, \quad (8)$$

where  $i$  is the index of images,  $W^{dino}$  and  $W^{dec}$  denote the similarity weights of features from DINO and decoder layers respectively, and  $S_i^{sim}$  is the average cosine similarity between them at the  $l$ -th decoder layer.  $S^{sim}$  is depicted in Figure 3, one can find that the similarity is lower for the shallow layers and higher for deep layers, indicating that **deeper layers are more conducive to learning semantic information.**

**Qualitative Analysis.** To provide further insights, we visualize the attention maps from decoder layers in Figure 4. In the first decoder layer, where  $S^{attn}$  is the highest and  $S^{sim}$  is the lowest, the attention maps exhibit very similar patterns for the very different images. Starting from the second layer, a gradual shift in attention behavior can be observed. As  $S^{attn}$  begins to decrease and  $S^{sim}$  increases, the attention maps demonstrate a transition

Decoder	FT Acc(%)
Transformer	82.9
Weighted Average	82.5
Conv Layer	82.9

Table 2. Comparisons of different decoders. As the decoder, single-layer convolution and weighted average exhibit effects akin to the transformer.

from focusing on fixed positions to adjacent foreground objects. This conclusion underscores the significance of a deep decoder for the efficacy of MAE’s pretraining, and aligns with the results of the ablation study about the decoder’s depth conducted in the original MAE paper [16] which demonstrated that a deeper decoder outperforms a shallower one in linear probing.

**The decoder mainly utilizes local features.** From Figure 4, another noteworthy observation is that the attention maps of mask tokens tend to focus more on nearby tokens. This implies that the decoder relies less on global image information for reconstruction, suggesting that local features are

adequate for MAE’s efficacy.

**Empirical Validation.** To validate this hypothesis, we replace the transformer-based decoder with operations that explicitly have a limited receptive field. Our first attempt is a nonparametric weighted average operation, in which the weights are set as a normalized two-dimensional Gaussian, with  $\sigma = 1$  and the size of the receptive field is about  $5 \times 5$ . A multi-layer perceptron (MLP) block is adopted to predict the masked pixels. We pretrain this *Weighted Average* decoder version and the original *Transformer* decoder version of MAE on ImageNet-1K [28] for 100 epochs using the same training strategy. As shown in Table 2, surprisingly, the *Weighted Average* decoder achieved a finetuning accuracy of 82.5%, which is only 0.4% lower than the *Transformer* decoder with much fewer parameters. Furthermore, we employ a convolutional layer with a kernel size of 5 as the decoder. We can see that this *Conv Layer* decoder achieves the same finetuning accuracy as the original MAE, reaching 82.9%. The result aligns with the previous observations and provides support for our interpretation of MAE’s decoder behavior: *local features within a limited region is sufficient for the decoder to reconstruct the image.*

## 4.2. Random Masking

In the local contrastive learning form of MAE, random masking acts as data augmentation, enabling MAE to learn invariance to missing image patches. From this perspective, the role of random masking is akin to random erasing [37]. However, even with complex self-supervised learning techniques, random erasing struggles to achieve the same level of effectiveness as random masking. It suggests that random masking provides additional benefits to MAE beyond just data augmentation.

### (1) Mask Ratio Controls The Effective Receptive Field.

We get started by considering the decoder’s attention maps. When without random masking, the most useful feature for reconstructing a patch’s pixels would be its own token. In this situation, the decoder would have no need to attend to other tokens. It is the random masking that forces the decoder to expand its receptive field to gather sufficient information for masked patch prediction.

Furthermore, the restricted receptive field of the decoder requires that the features output by the encoder are robust within local regions, implying that the encoder also primarily focuses on local features. To verify this, we compare the attention distance of MAE [16], DINO [5], and supervised pretrained DeiT[30]. Attention distance [10] is defined as the average distance between the query tokens and key tokens, multiplied by the attention weights. It is conceptually similar to the size of the effective receptive fields in CNNs. As illustrated in Figure 5, the attention distance of MAE is significantly lower than that of the contrastive learning

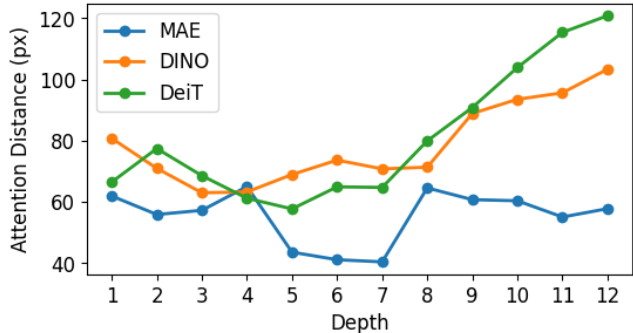


Figure 5. The attention distance for MAE, DINO, and DeiT. MAE’s attention distance is significantly smaller than that of the other pretraining methods.

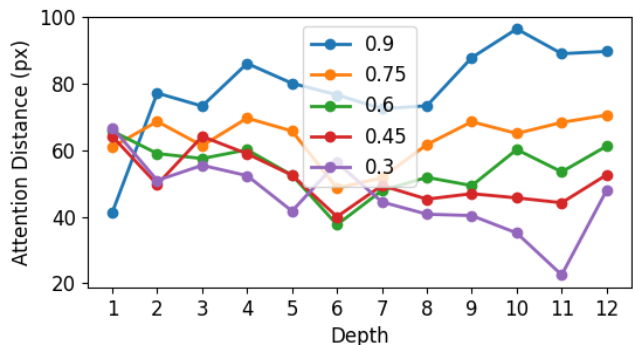


Figure 6. The attention distance for MAE across different mask ratios. There is a significant correlation between mask ratio and attention distance, a larger mask ratio leads to a greater attention distance.

method DINO and supervised pretrained DeiT, which validates the emphasis of MAEs on local information.

The intensity of random masking is controlled by the mask ratio. Intuitively, a smaller mask ratio permits the decoder to find features helpful for reconstruction within a narrower range, thereby indirectly controlling the size of the region for contrastive learning. We pretrain MAE on ImageNet-1K [28] for 100 epochs with mask ratios of 0.9, 0.75, 0.6, 0.45, and 0.3. The attention distances for different mask ratios are depicted in Figure 6. As we hypothesized, the mask ratio and attention distance exhibit a strong correlation, with the impact of mask ratio on attention distance being more pronounced in the deeper layers of the network. Specifically, a larger mask ratio results in a larger effective receptive field.

### (2) Limited Receptive Field Benefits Downstream Tasks.

As we discussed above, the role of random masking is twofold: acting as data augmentation and restricting the receptive field. In this part, we aim to clarify that the limited effective receptive field induced by random masking con-

Pretrain Methods	FT Acc(%)	LP Acc (%)
Random Init	78.6	-
MAE	82.9	55.4
AE(16)	78.7	5.7
AE(48)	81.2	5.7
AE(80)	81.5	5.6
AE(112)	81.8	5.6

Table 3. Finetuning accuracy (FT Acc) and linear probing accuracy (LP Acc) of ViT-B/16 pretrained by MAE and AutoEncoder (AE) on ImageNet-1K. The number in parentheses indicates the size of the image block each token reconstructs.

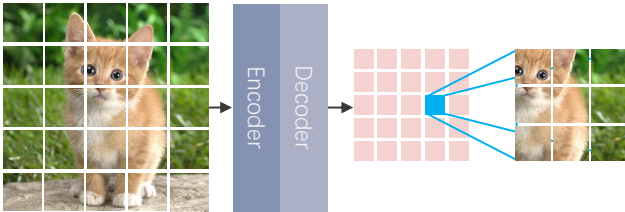


Figure 7. The overall architecture of autoencoder. Each token predicts an image block centered around itself. The image patches on the right are the ground truth for the token marked in blue.

tributes to the success of MAE on downstream tasks. In fact, previous works [22, 33, 35] have demonstrated that constraining the receptive field of vision transformers can accelerate convergence and enhance classification performance.

**Empirical Validation.** To isolate the effect of random masking as data augmentation and solely control the network’s receptive field, we make several modifications to MAE: 1) We discard the random masking operation, which degrades MAE to canonical AutoEncoder (AE); 2) We require each token to predict the pixel values of an image block centered around itself, which requires each token to focus on its surroundings, thus controlling the size of the receptive field. The overall architecture is shown in Figure 7.

We pretrain MAE and autoencoders on ImageNet-1K and evaluate their finetuning accuracy as well as their linear probing accuracy. The results are shown in Table 3. The patch size for ViT models is 16, so AE(16) represents MAE without random masking, while other versions of AE are autoencoders that have an increased size of image blocks to be predicted. Due to computational resource limitations, we do not use image block sizes larger than 112. When random masking is simply removed, the finetuning accuracy of MAE drops from 82.9% to 78.7%, which is similar to random initialization. When we enlarge the size of the target image block, the finetuning accuracy dramatically increases to 81.2% and peaks with a block size of 112, reach-

ing 81.8%. This suggests that the excellent finetuning accuracy of MAE is largely attributable to the appropriate receptive field afforded by random masking. However, the linear probing performance of all the autoencoders is poor, amounting to only about one-tenth of that achieved by the MAE (5.6% vs. 55.4%), indicating that the absence of random masking prevents the network from effectively learning semantic information.

In summary, random masking during pretraining (1) *augments training samples, enabling MAE to learn semantically meaningful representations*, and (2) *restricts the size of effective receptive fields, leading to MAE’s strong finetuning performance on downstream tasks*.

## 5. Experimental Details

**For pretraining**, we conduct experiments on the ImageNet-1K [28] training set, with ViT-B/16 [30] employed as the default backbone. For MAE pretraining, the mask ratio is set to 0.75 by default. We use AdamW [25] as the optimizer, with a batch size of 1024. The base learning rate  $base\_lr$  is initialized as  $1.5e-4$ , and the actual learning rate  $lr = base\_lr \times \frac{batch\_size}{256}$ . We adopt a 20-epoch linear warmup, and then the learning rate decays with the cosine scheduler [24]. For the pretraining of LC-MAE, we set the base learning rate to  $6e-4$ . The output dimension of the projector is set to 1024 by default.

**For finetuning**, all pretrained models employ the same strategy. We use the AdamW optimizer with a cosine decay learning rate schedule. The total training epoch number and the batch size are set to 100 and 1024, respectively. We set the base learning rate as  $1.0e-3$ , and use a 5-epoch warmup.

## 6. Conclusion

In this paper, we propose to understand MAE from a local perspective and introduce the local contrastive learning form of MAE. We design an empirical framework, Local Contrastive MAE (LC-MAE), to instantiate the contrastive learning form of MAE, which explicitly decomposes MAE’s training objective into a reconstruction loss and two contrastive losses in cross-view and in-view. With the two contrastive losses, we find that MAE inherently learns invariance to random masking and prevents collapse by constraining the distribution of the output feature vectors. We also delve into the roles of the two main components of MAE—decoder and random masking—in pretraining and summarize several useful designs, including (1) a deep decoder facilitates the learning of semantic information; (2) an appropriate receptive field size can improve finetuning accuracy for downstream tasks. We hope our findings can inspire future works to design more powerful self-supervised methods.



## References

- [1] Yuki M Asano, Christian Rupprecht, and Andrea Vedaldi. A critical analysis of self-supervision, or what we can learn from a single image. *arXiv preprint arXiv:1904.13132*, 2019. **1**
- [2] Hangbo Bao, Li Dong, Songhao Piao, and Furu Wei. Beit: Bert pre-training of image transformers. *arXiv preprint arXiv:2106.08254*, 2021. **1, 2**
- [3] Shuhao Cao, Peng Xu, and David A Clifton. How to understand masked autoencoders. *arXiv preprint arXiv:2202.03670*, 2022. **2**
- [4] Mathilde Caron, Ishan Misra, Julien Mairal, Priya Goyal, Piotr Bojanowski, and Armand Joulin. Unsupervised learning of visual features by contrasting cluster assignments. *Advances in neural information processing systems*, 33:9912–9924, 2020. **1, 2**
- [5] Mathilde Caron, Hugo Touvron, Ishan Misra, Hervé Jégou, Julien Mairal, Piotr Bojanowski, and Armand Joulin. Emerging properties in self-supervised vision transformers. In *Proceedings of the IEEE/CVF international conference on computer vision*, pages 9650–9660, 2021. **2, 5, 7**
- [6] Ting Chen, Simon Kornblith, Mohammad Norouzi, and Geoffrey Hinton. A simple framework for contrastive learning of visual representations. In *International conference on machine learning*, pages 1597–1607. PMLR, 2020. **2**
- [7] Xinlei Chen and Kaiming He. Exploring simple siamese representation learning. In *Proceedings of the IEEE/CVF conference on computer vision and pattern recognition*, pages 15750–15758, 2021. **2**
- [8] Xinlei Chen\*, Saining Xie\*, and Kaiming He. An empirical study of training self-supervised vision transformers. *arXiv preprint arXiv:2104.02057*, 2021. **1, 2**
- [9] Xiaokang Chen, Mingyu Ding, Xiaodi Wang, Ying Xin, Shentong Mo, Yunhao Wang, Shumin Han, Ping Luo, Gang Zeng, and Jingdong Wang. Context autoencoder for self-supervised representation learning. *International Journal of Computer Vision*, pages 1–16, 2023. **2**
- [10] Alexey Dosovitskiy, Lucas Beyer, Alexander Kolesnikov, Dirk Weissenborn, Xiaohua Zhai, Thomas Unterthiner, Mostafa Dehghani, Matthias Minderer, Georg Heigold, Sylvain Gelly, et al. An image is worth 16x16 words: Transformers for image recognition at scale. *arXiv preprint arXiv:2010.11929*, 2020. **2, 7**
- [11] Debidatta Dwibedi, Yusuf Aytar, Jonathan Tompson, Pierre Sermanet, and Andrew Zisserman. With a little help from my friends: Nearest-neighbor contrastive learning of visual representations. In *Proceedings of the IEEE/CVF International Conference on Computer Vision*, pages 9588–9597, 2021. **1, 2**
- [12] Alaaeldin El-Nouby, Hugo Touvron, Mathilde Caron, Piotr Bojanowski, Matthijs Douze, Armand Joulin, Ivan Laptev, Natalia Neverova, Gabriel Synnaeve, Jakob Verbeek, et al. Xcit: Cross-covariance image transformers. *arXiv preprint arXiv:2106.09681*, 2021. **2**
- [13] Peng Gao, Teli Ma, Hongsheng Li, Ziyi Lin, Jifeng Dai, and Yu Qiao. Convmae: Masked convolution meets masked autoencoders. *arXiv preprint arXiv:2205.03892*, 2022. **1**
- [14] Jean-Bastien Grill, Florian Strub, Florent Alché, Corentin Tallec, Pierre Richemond, Elena Buchatskaya, Carl Doersch, Bernardo Avila Pires, Zhaohan Guo, Mohammad Gheshlaghi Azar, et al. Bootstrap your own latent—a new approach to self-supervised learning. *Advances in neural information processing systems*, 33:21271–21284, 2020. **1, 2, 4**
- [15] Kaiming He, Haoqi Fan, Yuxin Wu, Saining Xie, and Ross Girshick. Momentum contrast for unsupervised visual representation learning. In *Proceedings of the IEEE/CVF conference on computer vision and pattern recognition*, pages 9729–9738, 2020. **1, 2**
- [16] Kaiming He, Xinlei Chen, Saining Xie, Yanghao Li, Piotr Dollár, and Ross Girshick. Masked autoencoders are scalable vision learners. In *Proceedings of the IEEE/CVF conference on computer vision and pattern recognition*, pages 16000–16009, 2022. **1, 2, 6, 7**
- [17] Zhicheng Huang, Xiaojie Jin, Chengze Lu, Qibin Hou, Ming-Ming Cheng, Dongmei Fu, Xiaohui Shen, and Jiashi Feng. Contrastive masked autoencoders are stronger vision learners. *arXiv preprint arXiv:2207.13532*, 2022. **2**
- [18] Lingjing Kong, Martin Q Ma, Guangyi Chen, Eric P Xing, Yuejie Chi, Louis-Philippe Morency, and Kun Zhang. Understanding masked autoencoders via hierarchical latent variable models. In *Proceedings of the IEEE/CVF Conference on Computer Vision and Pattern Recognition*, pages 7918–7928, 2023. **2**
- [19] Xiangwen Kong and Xiangyu Zhang. Understanding masked image modeling via learning occlusion invariant feature. In *Proceedings of the IEEE/CVF Conference on Computer Vision and Pattern Recognition*, pages 6241–6251, 2023. **1, 2, 3**
- [20] Gang Li, Heliang Zheng, Daqing Liu, Chaoyue Wang, Bing Su, and Changwen Zheng. Semmae: Semantic-guided masking for learning masked autoencoders. *Advances in Neural Information Processing Systems*, 35:14290–14302, 2022. **2**
- [21] Jihao Liu, Xin Huang, Yu Liu, and Hongsheng Li. Mixmim: Mixed and masked image modeling for efficient visual representation learning. *arXiv preprint arXiv:2205.13137*, 2022. **2**
- [22] Ze Liu, Yutong Lin, Yue Cao, Han Hu, Yixuan Wei, Zheng Zhang, Stephen Lin, and Baining Guo. Swin transformer: Hierarchical vision transformer using shifted windows. In *Proceedings of the IEEE/CVF international conference on computer vision*, pages 10012–10022, 2021. **8**
- [23] Zhengqi Liu, Jie Gui, and Hao Luo. Good helper is around you: Attention-driven masked image modeling. In *Proceedings of the AAAI Conference on Artificial Intelligence*, pages 1799–1807, 2023. **2**
- [24] Ilya Loshchilov and Frank Hutter. Sgdr: Stochastic gradient descent with warm restarts. *arXiv preprint arXiv:1608.03983*, 2016. **8**
- [25] Ilya Loshchilov and Frank Hutter. Decoupled weight decay regularization. *arXiv preprint arXiv:1711.05101*, 2017. **8**
- [26] Namuk Park, Wonjae Kim, Byeongho Heo, Taekyung Kim, and Sangdoon Yun. What do self-supervised vision transformers learn? *arXiv preprint arXiv:2305.00729*, 2023. **2**
- [27] Aditya Ramesh, Mikhail Pavlov, Gabriel Goh, Scott Gray, Chelsea Voss, Alec Radford, Mark Chen, and Ilya Sutskever.

- Zero-shot text-to-image generation. In *International Conference on Machine Learning*, pages 8821–8831. PMLR, 2021. [2](#)
- [28] Olga Russakovsky, Jia Deng, Hao Su, Jonathan Krause, Sanjeev Satheesh, Sean Ma, Zhiheng Huang, Andrej Karpathy, Aditya Khosla, Michael Bernstein, et al. Imagenet large scale visual recognition challenge. *International journal of computer vision*, 115:211–252, 2015. [7](#), [8](#)
- [29] Oriane Siméoni, Gilles Puy, Huy V Vo, Simon Roburin, Spyros Gidaris, Andrei Bursuc, Patrick Pérez, Renaud Marlet, and Jean Ponce. Localizing objects with self-supervised transformers and no labels. *arXiv preprint arXiv:2109.14279*, 2021. [5](#)
- [30] Hugo Touvron, Matthieu Cord, Matthijs Douze, Francisco Massa, Alexandre Sablayrolles, and Hervé Jégou. Training data-efficient image transformers & distillation through attention. In *International conference on machine learning*, pages 10347–10357. PMLR, 2021. [2](#), [7](#), [8](#)
- [31] Xudong Wang, Rohit Girdhar, Stella X Yu, and Ishan Misra. Cut and learn for unsupervised object detection and instance segmentation. In *Proceedings of the IEEE/CVF Conference on Computer Vision and Pattern Recognition*, pages 3124–3134, 2023. [5](#)
- [32] Yangtao Wang, Xi Shen, Yuan Yuan, Yuming Du, Maomao Li, Shell Xu Hu, James L Crowley, and Dominique Vaufreydaz. Tokencut: Segmenting objects in images and videos with self-supervised transformer and normalized cut. *IEEE Transactions on Pattern Analysis and Machine Intelligence*, 2023. [5](#)
- [33] Haiping Wu, Bin Xiao, Noel Codella, Mengchen Liu, Xiyang Dai, Lu Yuan, and Lei Zhang. Cvt: Introducing convolutions to vision transformers. In *Proceedings of the IEEE/CVF international conference on computer vision*, pages 22–31, 2021. [8](#)
- [34] Zhenda Xie, Zheng Zhang, Yue Cao, Yutong Lin, Jianmin Bao, Zhuliang Yao, Qi Dai, and Han Hu. Simmim: A simple framework for masked image modeling. In *Proceedings of the IEEE/CVF Conference on Computer Vision and Pattern Recognition*, pages 9653–9663, 2022. [1](#), [2](#)
- [35] Kun Yuan, Shaopeng Guo, Ziwei Liu, Aojun Zhou, Fengwei Yu, and Wei Wu. Incorporating convolution designs into visual transformers. In *Proceedings of the IEEE/CVF International Conference on Computer Vision*, pages 579–588, 2021. [8](#)
- [36] Qi Zhang, Yifei Wang, and Yisen Wang. How mask matters: Towards theoretical understandings of masked autoencoders. *Advances in Neural Information Processing Systems*, 35:27127–27139, 2022. [1](#), [2](#), [3](#)
- [37] Zhun Zhong, Liang Zheng, Guoliang Kang, Shaozi Li, and Yi Yang. Random erasing data augmentation. In *Proceedings of the AAAI conference on artificial intelligence*, pages 13001–13008, 2020. [7](#)
- [38] Jinghao Zhou, Chen Wei, Huiyu Wang, Wei Shen, Cihang Xie, Alan Yuille, and Tao Kong. ibot: Image bert pre-training with online tokenizer. *arXiv preprint arXiv:2111.07832*, 2021. [2](#)

## A. Additional Details of Autoencoders

One of the most important conclusions of our work is that the excellent finetuning performance of MAE is largely attributed to the limited receptive field brought by random masking. To substantiate this, in Table 3, we remove the random masking operation from MAE and attempt to control the size of the effective receptive field by adjusting the size of the predicted image blocks. The rationale behind this is that if the autoencoder aims to reconstruct the pixel values of an image block, its effective receptive field should at least cover this area.

In Figure A.1, we present the attention distance for autoencoders with different prediction sizes. It can be observed that the attention distance of the autoencoder with a prediction size of 16 is significantly smaller than that of other models. Meanwhile, by controlling the size of image blocks, the effective receptive field of the autoencoder can be effectively expanded.

However, the attention distances of the autoencoder and MAE exhibit different patterns: the attention distance of each layer in MAE is more stable, while autoencoders tend to learn a larger receptive field in the first two layers. This is because autoencoders have access to all patches, making it more efficient to expand the receptive field at the shallower layers. To further verify the contribution of restricting the receptive field to finetuning performance, following Asano et al. [1] and Kong and Zhang [19], we pre-train MAE using only a single image to limit its capacity to learn semantic information. The results, as shown in Table A.1, show that even when pretrained using a single image for 5 epochs, MAE achieves a finetuning accuracy of 81.8%, which is significantly higher than random initialization. Kong and Zhang [19] suggests that MAE learns a form of data-agnostic favored initialization, and we believe that this initialization is the restriction of the receptive field.

## B. More Visualizations

We provide more visualization of attention maps from decoder layers as shown in Figure B.1. As discussed in Section 4.1, the attention maps of the first decoder layer exhibit strong positional relevance, primarily focusing on the

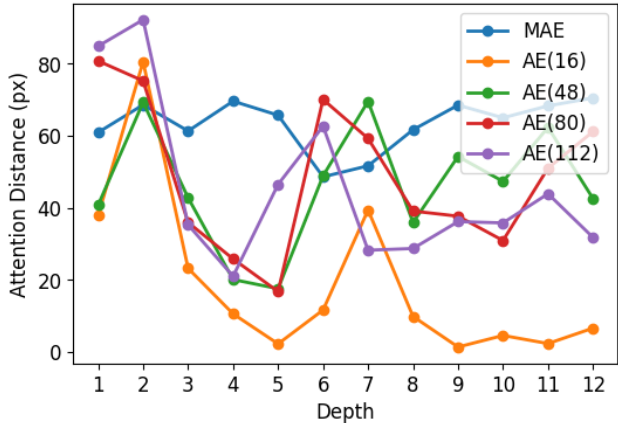


Figure A.1. The attention distance for MAE and AEs with different prediction sizes.

visible tokens surrounding the query token. The second layer shows a transition towards semantic relevance, and subsequent layers mainly focus on semantically related areas. Comparing different masked positions of the same image (first row vs. fourth row, second row vs. fifth row), we find that masked tokens pay more attention to their own surrounding local regions.

Pretrain Images	Pretrain Epochs	FT Acc(%)
1	5	81.8
ImageNet	100	82.9
Random Init	-	78.6

Table A.1. Comparisons of MAE pretrained with different numbers of images. “ImageNet” means using the whole training set of ImageNet for pretraining.

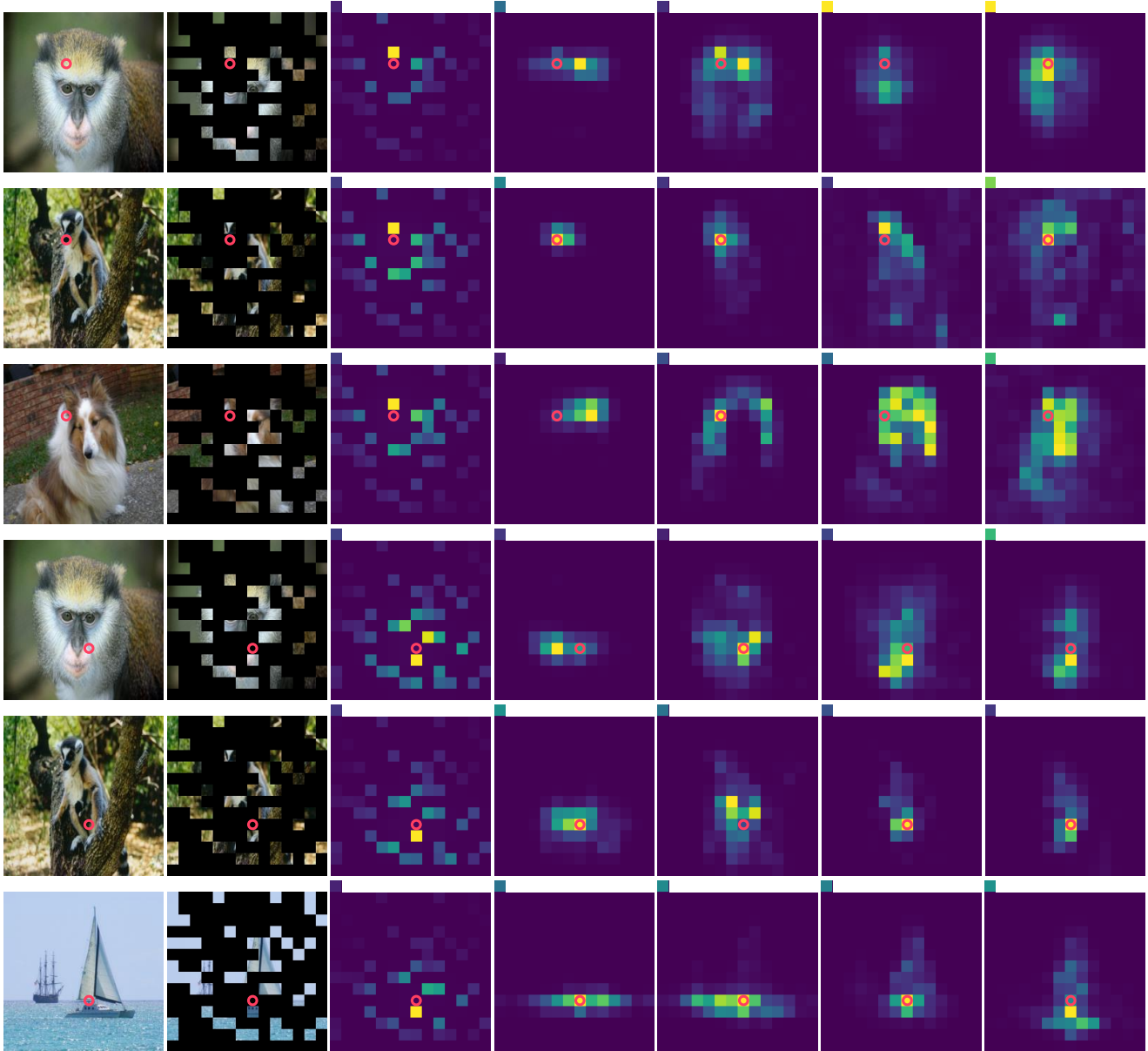


Figure B.1. Visualization of attention maps from decoder layers. From left to right: input images, masked images, and attention maps of the 1-st, 2-nd, 3-rd, 5-th, 8-th decoder layers. The red circles ( $\odot$ ) denote the masked tokens serving as queries. The block in the top-left of each attention map is the weight for the [CLS] token.